Open Access Online Journal on Astronomy and Astrophysics

Acta Astrophysica Taurica

www.astrophysicatauricum.org

Acta Astrophys. Tau. 7(2), 4–9 (2026) EDN: RQGMLN

Bauman Moscow State Technical University Radio Telescope RT-7.5: status and development prospects

V.V. Smirnova[1], V.B. Khaikin[2], G.A. Makoev[2], V.S. Ryzhov[3]

[1] Crimean Astrophysical Observatory, Nauchny 298409
e-mail: vvsvid.smirnova@yandex.ru
[2] Special Astrophysical Observatory RAS (Saint-Petersburg Department), Pulkovskoe sh. 65, Saint Petersburg 196140, Russia
e-mail: v_vkhstu@mail.ru
[3] Bauman Moscow State Technical University, 2-nd Baumanskaya 5, Moscow 105005, Russia
e-mail: v_vsryzhov@mail.ru

Received 6 October 2023

ABSTRACT

The paper describes the characteristics and current state of the Bauman Moscow State Technical University (BMSTU) millimeter radio telescope RT-7.5. We present the results of modeling in multi-beam operating mode at the RT-7.5. A concept of low-cost matrix receivers operating at the wavelengths of 3 and 2 mm is proposed, which can significantly reduce the time needed to obtain solar maps. The expected model images of solar subterahertz flares with a positive spectral slope at 3 and 2 mm are presented.

Key words: Sun, radio telescope, multi-beam operating mode, matrix receivers, solar flares, millimeter radio emission, chromosphere

1 Introduction

One of the important scientific tasks in the millimeter radio wavelength range is the study of solar flares during which powerful energy release, particle acceleration, and plasma ejections occur, significantly affecting the state of interplanetary space and Earth's magnetic field. The task is topical because observational data on flares in the 2–4 mm wavelength range are currently very scarce and inhomogeneous (Smirnova et al., 2016). At the same time, these data may contain unique information on the characteristics of high-energy electron fluxes with energies > 1 MeV, physical parameters of the plasma, and location of the flare energy release source. Moreover, the nature of emission from solar sub-THz flares with a positive spectral slope is not yet fully understood (Tsap et al., 2016).

Obtaining radio intensity distribution maps of the solar disk with the RT-7.5 via scanning takes 5–8 minutes. Such maps are important for studying long-period variations of the quiet chromosphere but are unsuitable for investigating non-stationary flare processes that typically last only a few minutes. Therefore, the possibility of obtaining solar disk maps as rapidly as possible without losing time for scanning is an important task.

The work aims to explore the operation of the RT-7.5 in multi-beam mode with a matrix receiver at the secondary focus and simulate the expected images of solar sub-THz flares at the wavelengths of 3 and 2 mm (93 and 140 GHz) using the proposed matrix receivers. The solution of this problem is of both astrophysical and methodological interest, in particular for tasks related to adjusting matrix operating modes of the millimeter telescope. It is proposed to apply such methods to the Eurasian Submillimeter Telescopes (ESMT; Khaikin et al., 2020) using the RT-7.5 as a laboratory for searching for optimal approaches to this task.

2 Main characteristics of the RT-7.5

2.1 Feed system

The BMSTU RT-7.5 radio telescope is designed for operation in the short-wavelength part of the millimeter range (1–4 mm) and is among large solar radio telescopes operating in this range (Shustikov et al., 2012). The radio telescope is located near Dmitrov (Moscow region). The 7.75-m antenna is equipped with a dual-frequency receiving system currently installed at the primary focus, which enables simultaneous observations at 3.2 and 2.2 mm (93 and 140 GHz) wavelengths, with beam widths of 2.5′ and 1.5′, respectively. A high-precision synchronous tracking drive ensures tracking of astronomical objects. The high fluctuation sensitivity of the receiving system (0.1 K brightness temperature and 0.01 s.f.u. flux), together with a high temporal resolution of 0.125 s, allows a number of topical scientific tasks to be solved, the principal one of which is the study of the solar chromosphere (Shustikov et al., 2015).

Two feed systems are possible for the RT-7.5 antenna: from the primary and secondary foci. The decision to transit to a dual-reflector feed system for the RT-7.5 antenna was made due to the development of a dual-band receiver for the radio telescope. The illumination angle of the mirror from the primary focus is $2\phi\nu = 120°$ (Fig. 1), which rules out the applying of quasi-optical methods for combining beams at 2.2 and 3.2 mm wavelengths on the primary mirror axis of the radio telescope.

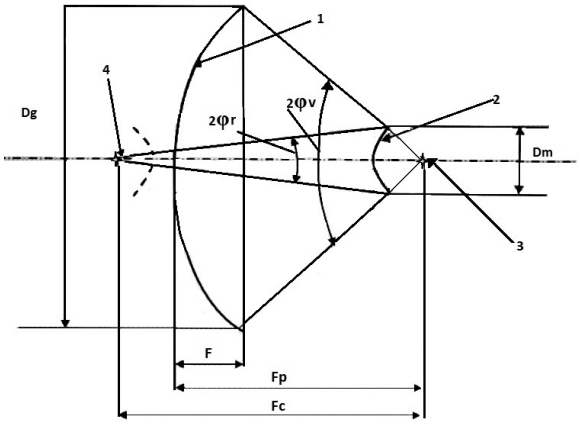

Fig. 1. Feed system layout of the BMSTU RT-7.5 radio telescope from the secondary focus.

The detailed feed system layout of the RT-7.5 is presented in Fig. 1. Here: 1 – primary mirror, 2 – subreflector, 3 – primary focus position, 4 – secondary focus position. The letter designations are as follows: $D_g = 7.75$ m – diameter of the primary mirror, $F_p = 3.25$ m – focal length of the paraboloid of revolution, $F_c = 3.75$ m – distance between the foci of the hyperbola, F – depth of the primary mirror dish, $D_m = 600$ mm – diameter of the subreflector.

The chosen Cassegrain dual-reflector design satisfies the requirements for the divergence of the primary feed beams, leads to a decrease in the antenna noise temperature, and provides the possibility of placing the receivers for both bands near the secondary focus located behind the primary mirror. It involves the use of a hyperbolic reflector (subreflector) as the secondary mirror, which, together with the parabolic primary mirror, forms a plane phase front of the electromagnetic wave. The illumination angle of the subreflector from the secondary focus is $2\phi_r = 8°$, yielding the magnification $M = 15$ for the antenna system.

2.2 Reflecting surface quality and gain of the RT-7.5 antenna

Errors of the reflecting surface of parabolic antennas are the main source of their reduced efficiency, and they determine the minimum wavelength at which they can operate effectively. These errors have different origins and spatial scales and affect the electrical characteristics of the antenna in different ways. Gravitational large-scale deformations are functionally related to the antenna slope angle; thermal large-scale deformations, to the antenna orientation relative to the Sun, gradients of the ambient temperature, and the backup structure; and small-scale deformations, to the temperature

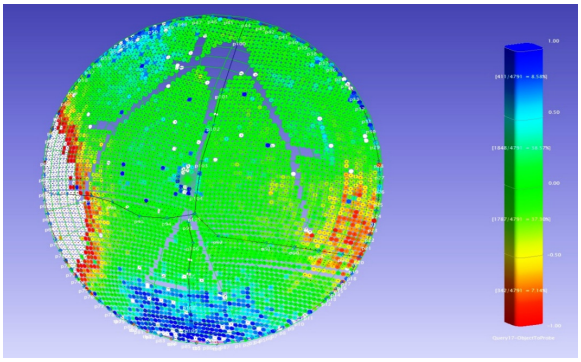

(a)

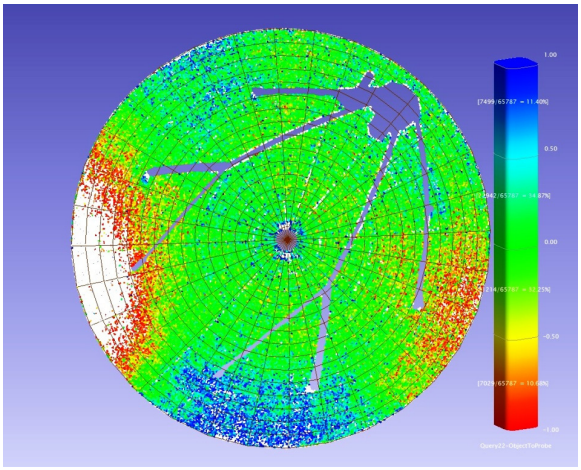

(b)

Fig. 2. Results of the RT-7.5 antenna surface RMS error measurements: (a) measurements with the MV 224 radar, (b) measurements with the Z+F IMAGER laser.

gradients on the panels themselves. These errors give rise to distortions of the beam pattern shape, growth of sidelobes, and a loss of gain. Panel manufacturing errors are typically small and random. In addition, errors in the mutual alignment of panels must be taken into account. The aforementioned surface errors lead to increased scattering into far sidelobes and an overall decrease in the antenna gain G. According to the Ruze formula (Ruze, 1966), this decrease has exponential nature:

$$G = G_0 exp\left(\frac{-4\pi\sigma}{\lambda}\right)^2, \quad (1)$$

where $G_0 = (\frac{\epsilon_0 \pi^2 D_g^2}{\lambda})^2$ is the gain of the same antenna with an ideally accurate surface; σ is the root-mean-square (RMS) surface error; λ is the wavelength. The aperture coefficient ϵ_0 is related to occultation, non-uniform illumination, under-/over-illumination of the antenna, etc. (for properly illuminated antennas ϵ_0 is no less than 0.75). However, the widely used Ruze formula given above has a number of constraints. In particular, it does not account for the following circumstances:

– surface errors of the antenna are random in nature and uniformly distributed over the aperture;
– surface errors are distributed within fixed circular correlation regions;
– the antenna aperture is significantly larger than the possible error correlation radius C related to the panel size ($D_g \gg 2C$);
– surface errors have a Gaussian spatial phase correlation.

Furthermore, for an arbitrary F_p/D_g, the Ruze correction factor A must be taken into account; it is included into the exponent of the equation $\frac{G}{G_0} = e^{-A(4\pi\sigma/\lambda)^2}$ multiplicatively, where $A = 0.8$–1.0 for $F_p/D_g = 0.4$–1.0 (Ruze, 1966).

Since G_0 increases as λ^2 with decreasing wavelength, while at the same time the second factor in (1) decreases exponentially, there exists a wavelength λ_0 at which the antenna gain is maximal.

Figure 2 presents the results of RMS error measurements of the RT-7.5 antenna surface obtained through laser geodesy methods using instruments that had been previously successfully tested in collaboration with Neva Technology LLC on the parabolic secondary mirror of the RATAN-600 radio telescope, with RMS = 0.31 mm (Khaikin et al., 2013).

The RT-7.5 surface was scanned contactlessly using the MV 224 radar and the Z+F IMAGER scanner.

Results of the MV 224 radar scanning (Fig. 2a):

– theoretical focal length is 3250 mm; focal length obtained from the scanning results is 3253 mm;
– RMS error of the entire paraboloid surface is 0.34 mm;
– RMS error of the central part of the paraboloid surface with a diameter of 5 m is 0.16 mm. Maximum deviations from the paraboloid surface are up to 2 mm (white zone on the deviation map).

Results of the Z+F IMAGER scanning (Fig. 2b):

– theoretical focal length is 3250 mm; focal length obtained from the scanning results is 3252.80 mm;
– RMS error of the entire paraboloid surface is 0.37 mm. Maximum deviations from the paraboloid surface are up to 2 mm (white zone on the deviation map).

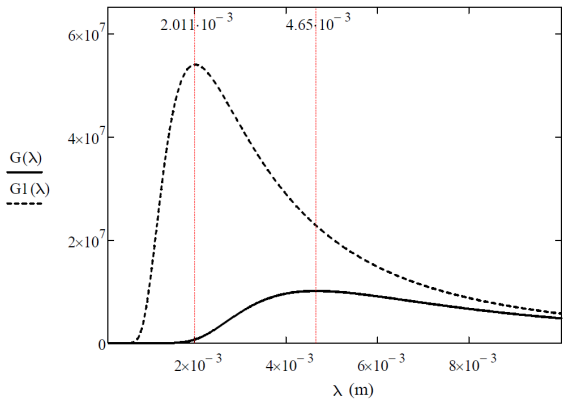

Fig. 3. Results of calculating $G(\lambda)$ with RMS = 0.34 mm for the entire RT-7.5 antenna and $G1(\lambda)$ with RMS = 0.16 mm for its central part.

Taking into account the RMS error of the RT-7.5 antenna surface, we calculate the minimum wavelength at which the antenna gain is maximal for the full aperture and its central part (5 m). To this end, we plot $G(\lambda)$, taking into account the measured RMS error of the full aperture surface and its central part (Fig. 3).

It can be seen that for the full aperture, the maximum gain $G(\lambda)$ is observed at a wavelength of 4.6 mm, whereas when using the central part of the primary mirror, the maximum gain $G1(\lambda)$ is achieved at a wavelength of ~2 mm. This explains why at present only the central part of the aperture is illuminated at the RT-7.5, which yields the maximum value of G, leading to a substantial decrease in the half-power beam width of the antenna at both wavelengths.

2.3 Calculated and experimental beam patterns of the RT-7.5 antenna

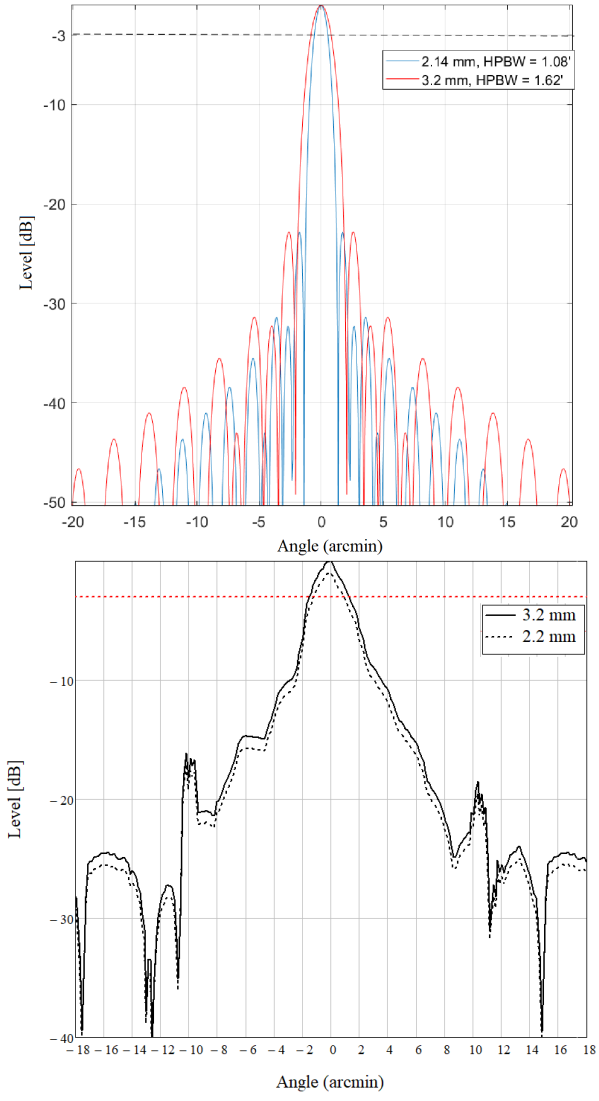

Fig. 4. Top: calculated BP of the RT-7.5 antenna for two wavelengths. Bottom: BP of the RT-7.5 antenna obtained using solar measurements. The horizontal dashed line on both panels corresponds to the −3 dB level.

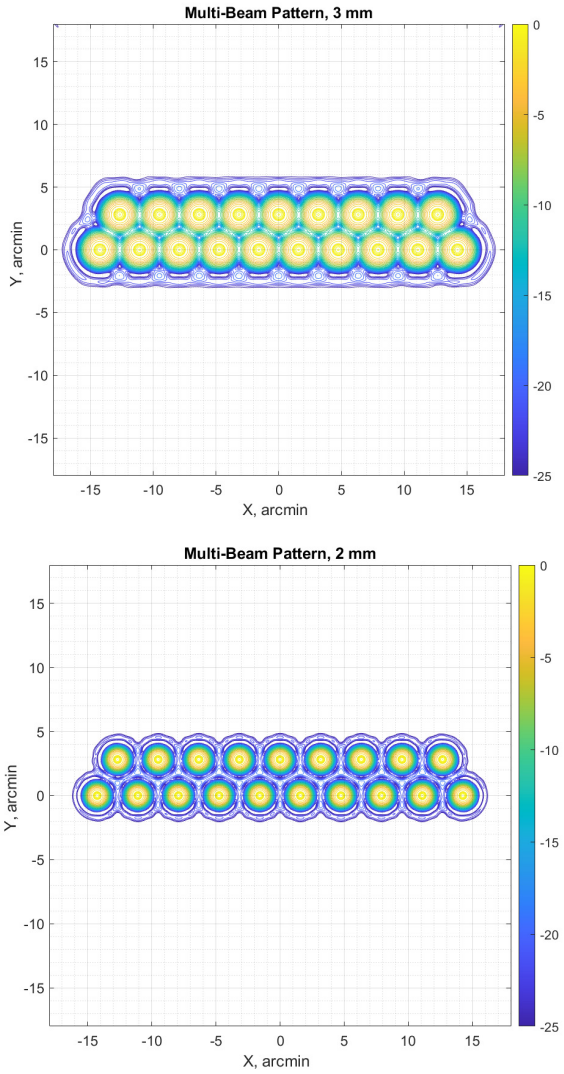

Fig. 5. Calculated two-dimensional BPs of the RT-7.5 for two-row 10 + 9 beam matrices. Top: for a wavelength of 3.2 mm. Bottom: for a wavelength of 2.2 mm.

The receiving system of the RT-7.5 comprises two radiometers operating at 93 and 140 GHz. The beam pattern (BP) of the RT-7.5 at these frequencies was calculated using the method for direct integration of the aperture field, previously described in Khaikin, Makoev (2023). The results of the BP calculation are presented in Fig. 4. It can be seen that at the −3 dB level, the beam patterns are fairly narrow, with widths of 1.6 and 1.1 arcmin at 93 and 140 GHz, respectively. The BP calculation was performed for the full antenna aperture with optimal illumination.

The bottom panel of Fig. 4 shows the antenna beam pattern obtained using solar measurements, which is ∼2.5′ at both frequencies. The measurements were carried out in 2019 using the method for solar map processing. The solid and dashed lines represent the BPs at 93 and 140 GHz, respectively. The broader BP of the RT-7.5 compared to the calculated one is a consequence of under-illumination of the primary mirror aperture due to significant edge distortions.

3 Modeling of multi-beam patterns of the RT-7.5 and expected images of sub-THz solar flares

As already noted, scanning of the solar disk (construction of a full map during observations) with the RT-7.5 currently takes 5–8 minutes, which is insufficient for studying non-stationary flare processes that may occur within a few minutes (Ryzhov et al., 2023). When tracking a local active region (AR), other ARs in which dynamics leading to a flare may occur remain unmonitored. Accordingly, during both scanning and tracking of a region, an important part of the information on the behavior of sub-THz emission is lost.

To advance the receiving system of the RT-7.5, matrix receivers can be applied, which are actively used in modern radio astronomy, allowing one to eliminate the scanning method. In this case, the image of the object under study is obtained almost instantaneously. However, a significant drawback of the matrix receiver is its high cost associated with a large number of receiving elements, each of which is a compact radiometer with a compact horn. Therefore, a more cost-effective version of a closely packed two-row matrix has been proposed for the RT-7.5. With such a matrix, the solar scanning time along one coordinate is 1–2 s.

Using the method described in Khaikin, Makoev (2023), multi-beam BPs of the RT-7.5 were simulated for two-row 10 + 9 element matrices placed at the secondary focus. The calculated multi-beam BPs of the RT-7.5 obtained with such matrices are presented in Figs. 5 and 6. As expected, for a matrix of this size, the off-axis aberrations of the BP in the Cassegrain double-reflector configuration with the magnification $M \sim 15$ become negligible. It was also shown in Khaikin, Makoev (2023) that at $M = 12.5$ not only coma but also other field aberrations are insignificant, except for the image field curvature limiting the applicability of plane-wave matrices with a size of 9×9 elements at a wavelength of 1 mm and shorter.

A folding of the solar model with the calculated multi-beam BPs was performed to estimate the quality of the images obtained during fast scanning of the solar disk. The model incorporated local sources that are fairly compact relative to the BP half-power width (no larger than the BP size) and a disk-shaped source of 4′ in diameter corresponding to a typical AR, as well as sources in the form of flare ribbons with an area of about 1000 $(\text{arcsec})^2$. Following Kontar et al. (2018), it was assumed that the source of thermal sub-THz emission from solar flares with a positive slope of the spectrum may be flare ribbons with temperatures of 10^4–10^6 K. The quiet Sun was specified as a uniform intensity disk with limb brightening (Borovik, 1997). The brightness temperature of the quiet Sun was set according to the formula $T_b = 5950 \cdot \lambda^{0.16}$ (Pelyushenko, 1982).

Figure 7 presents the results of folding the solar model that includes compact optically thick sources ($T_b = T = 10^5$ K) and an AR ($T_b = T = 3 \times 10^4$ K) with the previously obtained idealized multi-beam BPs of the RT-7.5 (without accounting for surface errors) for a two-row matrix. On the expected images, the bright compact sources and the disk-shaped ARs are clearly visible. The vertical elongation of the images of circularly symmetric compact sources reflects the result of their vertical folding with the two-dimensional BP of the RT-7.5.

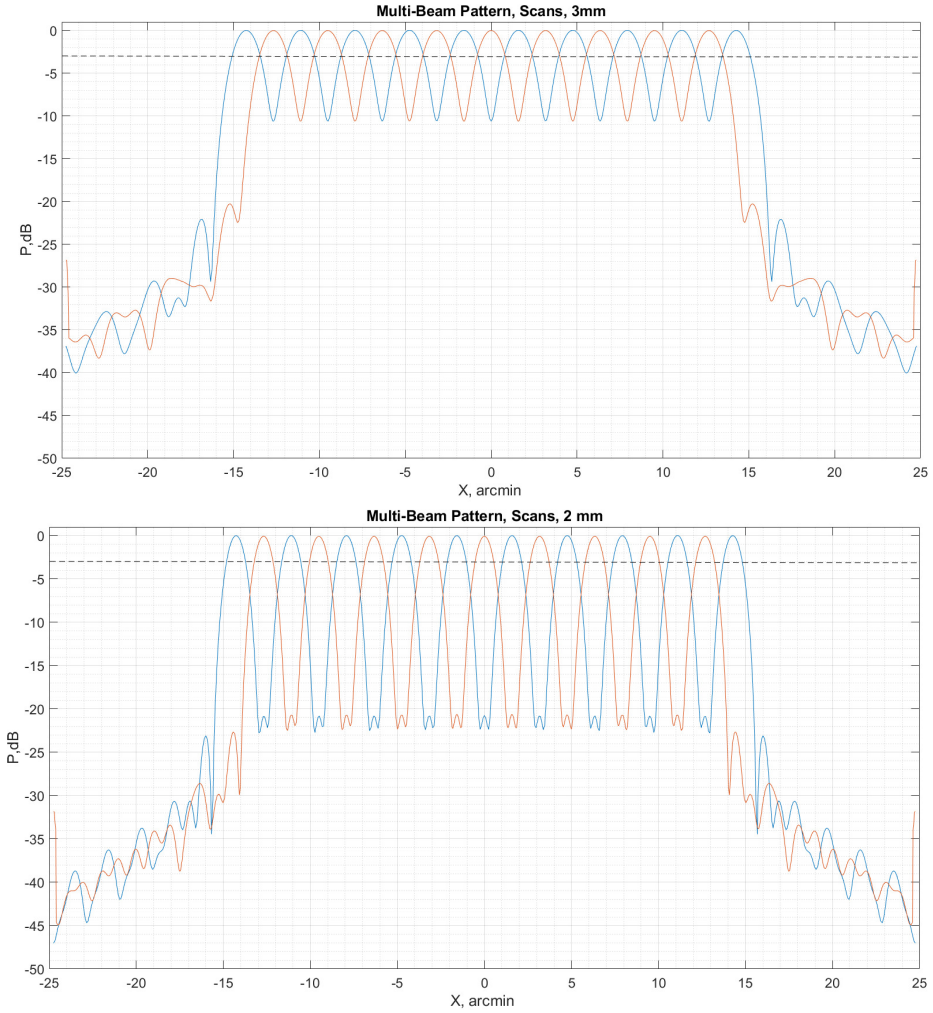

Fig. 6. Calculated one-dimensional BPs of the RT-7.5 for two-row 10 + 9 beam matrices. Top: for a wavelength of 3.2 mm. Bottom: for a wavelength of 2.2 mm.

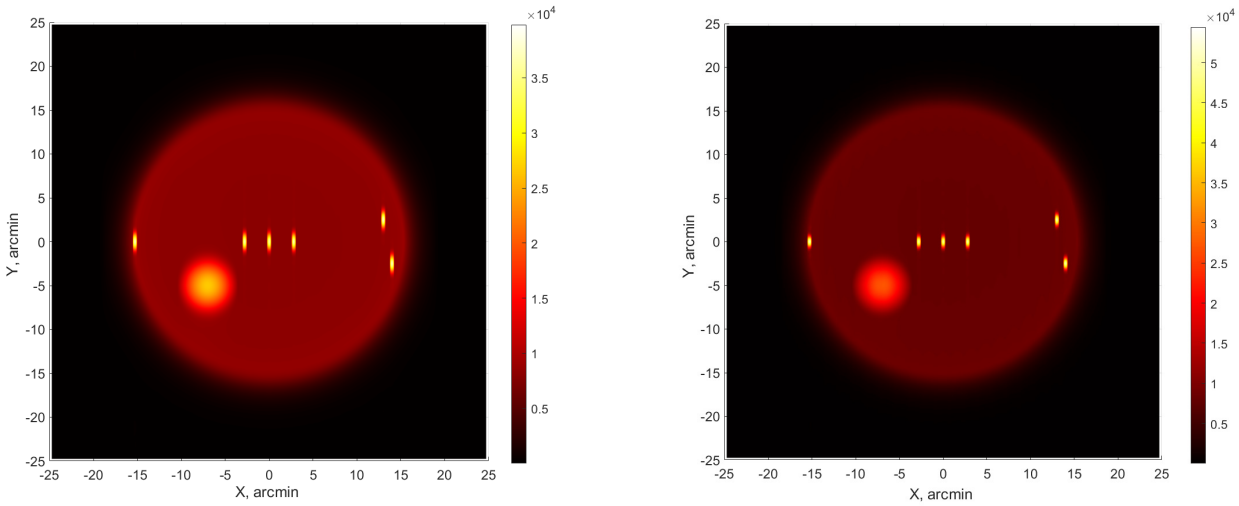

Fig. 7. Folding the solar model with the calculated multi-beam BPs. Left: for a wavelength of 3.2 mm. Right: for a wavelength of 2.2 mm.

4 Conclusions

Effective studies of solar activity in the short millimeter wavelength range are currently conducting at the RT-7.5. One of the constraints on studying non-stationary processes on the Sun with the RT-7.5 is the slow construction of solar disk maps in single-beam mode.

We have performed modeling of the multi-beam operating mode of the RT-7.5. The results obtained demonstrate that matrix receivers are able to significantly enhance the efficiency of the RT-7.5. In this case, scanning of the Sun along one coordinate takes 1–2 s, which enables the study of the dynamics of all active regions observed on the solar disk, leading to the detection of a considerably larger number of sub-THz events.

The work was supported by the RFBR grant 20-52-26006 Czech Republic_a (V.V. Smirnova), the RSF grant 23-72-00041 (G.A. Makoev), and partially supported by the Ministry of Science and Higher Education, research project No. 1021051101548-7-1.3.8.

References

Borovik V.N., 1997. Study of the quiet Sun in the microwave range on the RATAN-600 and BPR radio telescopes in the XX-XXII solar activity cycles, PhD thesis. Nizhnij Arkhyz: Astrofizika, radioastronomiya. (In Russ.)

Ryzhov V.S., Shivrina P.V., Smirnova V.V., 2023. Izv. Krymsk. Astrofiz. Observ., vol. 119, no. 1, pp. 11–18. (In Russ.)

Khaikin V.B., Makoev G.A., 2023. Trudy IPA RAN, in press. (In Russ.)

Khaikin V.B., Bursov N.N., Vikoruk D.G., Druzinin M.Y., Yakovlev S.V., Kornev A.V., 2013. Proceedings of the 7th European Conference on Antennas and Propagation, pp. 4090–4099.

Khaikin V., Lebedev M., Shmagin V., Zinchenko I., Vdovin V., et al., 2020. Proceedings of the 7th All-Russian Microwave Conference, pp. 47–51.

Kontar E.P., Motorina G.G., Jeffrey N.L.S., Tsap Y.T., Fleishman G.D., Stepanov A.V., 2018. Astron. Astrophys., vol. 620, id. A95, pp. 1–6.

Pelyushenko S.A., 1982. Radiophys. Quantum. Electron., vol. 25, no. 11, pp. 906–913.

Ruze J., 1966. Proceedings of the IEEE, vol. 54, no. 4, pp. 633–640.

Shustikov V.Y., Shumov A.V., Ryzhov V.S., Zhiltsov A.V., 2012. Vestnik MGTU im. N.E. Baumana. Priborostroenie, no. 7, pp. 277–288. (In Russ.)

Shustikov V.Y., Shumov A.V., Tsap Y.T., Zharkova N.A., Morgachev A.S., et al., 2015. Nauka i Obrazovanie. MGTU im. N.E. Baumana, no. 9, pp. 106–121. (In Russ.)

Smirnova V.V., Tsap Y.T., Shumov A.V., Morgachev A.S., Motorina G.G., et al., 2016. Nauka i Obrazovanie. MGTU im. N.E. Baumana, no. 12, pp. 85–97. (In Russ.)

Tsap Yu.T., Smirnova V.V., Morgachev A.S., Motorina G.G., Kontar E.P., et al., 2016. Advances in Space Research, vol. 57, iss. 7, pp. 1449–1455.